Characterization of Intermetallic Diffusion Barrier and Alloy Formation for Pd/Cu and Pd/Ag Porous Stainless Steel Composite Membranes

ARTICLE *in* INDUSTRIAL & ENGINEERING CHEMISTRY RESEARCH · DECEMBER 2003

Impact Factor: 2.59 · DOI: 10.1021/ie034002e

6 AUTHORS, INCLUDING:

Yi Hua Ma
Worcester Polytechnic Institute
96 PUBLICATIONS **2,318** CITATIONS
SEE PROFILE

Engin Ayturk
13 PUBLICATIONS **297** CITATIONS
SEE PROFILE

Federico Guazzone
Worcester Polytechnic Institute
21 PUBLICATIONS **283** CITATIONS
SEE PROFILE

Ivan P. Mardilovich
Worcester Polytechnic Institute
64 PUBLICATIONS **478** CITATIONS
SEE PROFILE

Characterization of Intermetallic Diffusion Barrier and Alloy Formation for Pd/Cu and Pd/Ag Porous Stainless Steel Composite Membranes

Yi Hua Ma,* B. Ceylan Akis, M. Engin Ayturk, Federico Guazzone, Erik E. Engwall, and Ivan P. Mardilovich

Center for Inorganic Membrane Studies, Department of Chemical Engineering, Worcester Polytechnic Institute, Worcester, Massachusetts 01609

The formation of the intermetallic diffusion barrier layer by the controlled in-situ oxidation method for Pd and Pd/alloy porous stainless steel composite membranes was investigated. SEM and EDS results showed the existence of an oxide layer as the intermetallic diffusion barrier for oxidation temperatures higher than 600 °C. At oxidation temperatures lower than 600 °C, there might still be an oxide layer at the membrane−substrate interface although it was too thin to be detected by SEM and EDS. The alloy formation study showed that annealing at 500 °C under helium atmosphere did not produce alloys with uniform compositions either for Pd/Ag or Pd/Cu membranes. However, annealing at 600 °C gave a uniform Pd/Cu−porous stainless steel (PSS) composite membrane, with no detectable presence of elements from the PSS substrate, further demonstrating the oxide layer as an effective intermetallic diffusion barrier.

1. Introduction

Currently, approximately 11 million tons of hydrogen are produced every year in the U.S. At the present, hydrogen is mainly used in the petrochemical industry and only a small amount is used as fuel in the space industry. However, hydrogen production is expected to increase since hydrogen will be widely used as a fuel in the "hydrogen economy" of the 21st century. An annual production of 40 million tons was estimated by the United States Department of Energy to sustain 100 million fuel-cell powered cars or 25 million homes.[1]

Steam re-forming of hydrocarbons is the most cost-effective process for hydrogen production and accounts for 95% of the total hydrogen produced in the United States. However, steam re-forming is considered to be the transitional process between a hydrocarbon-based hydrogen production and a carbon-free-based hydrogen production where solar and probably nuclear energy will play an important role. According to Barreto et al.,[2] steam re-forming will still be preferentially used in the United States, Western Europe, Eastern Europe, and the former Soviet Union until 2100 for the production of hydrogen. Although the usual conversion in the steam re-forming process at 500 °C is around 20%,[3] the methane conversion can be increased up to 99% in a membrane reactor including a Pd or Pd alloy composite membrane.[4,5]

Pd and Pd alloy composite membranes have been extensively investigated by several authors.[6−12] A better understanding of the physical properties of the interface between the Pd film and porous substrate is important in obtaining thermally stable composite Pd and Pd/alloy membranes. SEM was used by Uemiya et al.[6] to follow structural changes at every step during the Pd/Ag membrane synthesis to investigate the alloying process of Pd and Ag. They concluded that annealing at 500 °C for 12 h did not lead to a homogeneous Pd/Ag alloy phase and that a higher temperature would be required. Shu et al.[13] also used SEM to show the preferential deposition of Ag on the surface of the porous stainless steel (PSS) substrate, leaving the pores uncovered. Li et al.[14] investigated the synthesis of a Pd/Ag membrane by the spray pyrolysis method. They showed that small islands were formed at the beginning of the process and only combined after 100 min of plating to form a continuous Pd/Ag film. Cheng and Yeung[9] used SEM to investigate the microstructure of electroless deposited Pd on Vycor glass at different stages of the process and concluded that nucleation and growth took place simultaneously. They also observed an increase in Pd cluster size as a function of time. Souleimanova et al.[15] also used SEM to study the effect of osmotic pressure on Pd morphology and reported the formation of finer Pd particles at high osmotic pressures. Edlund et al.[16] examined the vanadium concentration profile from a cross section of an annealed palladium vanadium interface and showed that intermetallic diffusion occurred at a higher rate in the presence of hydrogen than in an inert atmosphere. Little work has been done on the Pd/Cu system. This is due, in part, to the fact that, at its optimum Cu concentration, Pd/40 wt % Cu, the permeability of the alloy is only 1.1 times the permeability of pure Pd.[17] However, the Pd/40 wt % Cu alloy does not undergo any α to β transformation even at room temperature since its $p-C$ isotherm at 25 °C does not show any invariance in pressure.[18] Therefore, Pd/Cu is one of the most robust systems toward hydrogen embrittlement and temperature cycling available for hydrogen purification processes. There has also been some interest in the H_2S resistance of Pd/Cu membranes.[19] Uemiya et al.[6] and Roa et al.[20] reported Pd/ 40 wt % Cu alloy membranes, supported on ceramic supports, with a permeability slightly lower than that of pure Pd.

Although porous stainless steel has been used as the substrate for composite Pd membranes,[13,21] the preferred substrates reported in the literature appear to

10.1021/ie034002e CCC: $27.50
Published on Web 12/18/2003

be ceramic and Vycor glass. The main differences between Pd/PSS and Pd/ceramic membranes are the thickness of dense Pd layers that can be achieved and the temperature range at which the membranes can be operated. Indeed, the thickness of a dense Pd film depends strongly on the morphology, roughness, and size of the largest pores of the substrate surface. Ceramics may be synthesized with a relatively smooth surface layer containing very uniform small pore systems. Therefore, very thin dense Pd membranes can be obtained (e.g., 1−6 μm) using ceramic supports. Furthermore, since there is no intermetallic diffusion between the ceramic support and the Pd layer, the formation of an alloy can be achieved at higher temperatures. On the other hand, there are a number of advantages for using PSS supports, including better mechanical strength, operation at high pressures, resistance to cracking, ease of module fabrication and sealing, and, finally, similar thermal expansion coefficients of Pd and PSS resulting in better mechanical properties of the membrane during temperature cycling.

To reduce intermetallic diffusion between the metal support and Pd layer, thereby improving the stability of the Pd/PSS composite membranes, Ma et al.[22] developed a controlled in-situ oxidation of the porous stainless steel prior to plating to produce an oxide layer to act as a diffusion barrier between the Pd and the PSS. Membranes produced by this method have been shown to be stable for over 6000 h in the temperature range of 350−450 °C.[23]

The objective of this study was to investigate the effects of temperature on the formation of the intermetallic diffusion barrier layer by the controlled in-situ oxidation method for Pd and Pd/alloy porous stainless steel composite membranes using SEM and EDS. In addition, the effects of the annealing temperature on the alloy formation of Pd/Ag and Pd/Cu porous stainless steel composite membranes were also studied with barrier layers formed at different temperatures to ascertain the effectiveness of the barrier layer to minimize the intermetallic diffusion. The obtained information provided a better understanding of the intermetallic diffusion at the interface between the membrane layer and the metal substrate, which is essential for making a composite Pd and Pd/alloy porous stainless steel membrane with long-term thermal stability.

2. Experimental Section

2.1. Membrane Supports and Chemicals. Both porous stainless steel plates (PSS plates) and cups were used. PSS plates were prepared by cutting 1 dm^2 316L 0.5 μm grade PSS sheets into 1 cm^2 pieces. Cups were 0.5 μm grade 316L PSS cylinders which were 2.5 cm long and 1.17 cm in diameter and were sealed at one end with the same porous material as the cylinder wall. Both porous plates and cups were purchased from Mott Metallurgical Corp.

The support grades are determined by Mott using the ASTM E-128 standard procedure, which relates capillary size to the pressure drop required to expel a liquid from the pore using a gas.[24] Previous work in this laboratory has shown that the pore sizes for PSS supports obtained by Hg porosimetry are somewhat larger than the support grade reported by the manufacturer.[25] Mercury porosimetry analysis of a 0.5 μm grade cup resulted in a distribution of pores ranging from 1 to 12 μm in diameter. Also, large pores (10−20 μm) could be found on the surface of the porous supports.

Table 1. Chemical Compositions of the Plating Solutions

	Pd bath	Ag bath	Cu bath
$Pd(NH_3)_4Cl_2 \cdot H_2O$ (g/L)	4		
$AgNO_3$ (g/L)		0.519	
$CuSO_4 \cdot 5H_2O$ (g/L)			20
$Na_2EDTA \cdot 2H_2O$ (g/L)	40.1	40.1	30
NH_4OH (28%) (mL/L)	198	198	
H_2NNH_2 (1 M) (mL/L)	5.6	5.6	
HCHO (37%) (mL/L)			14
EDA (ppm)			100
$K_4Fe(CN)_6 \cdot 3H_2O$ (ppm)			35
$(C_2H_5)_2NCS_2Na \cdot 3H_2O$ (ppm)			5
pH	10−11	10−11	12−13
temp (°C)	60	60	20−25

PSS supports were cleaned before activation and electroless deposition of metals. The following cleaning procedure was used for every sample. The samples were immersed for 30−60 min in an alkaline solution, including 5 mL/L of a saturated solution of industrial detergent, for dirt and grease removal. The samples were then thoroughly washed with high purity water (DI water) to remove the basic solution trapped in the pores of the supports. A strip of pH paper was touched to the wet surface of samples to check the pH of the liquid remaining within the pores. The DI water rinse step was ended only after reaching a pH of 7. The last cleaning step involved a 10 min immersion in 2-propanol to ease the drying of the supports. All cleaning steps were carried out in ultrasonic bath at 60 °C. The supports were finally dried at 120 °C for 2−4 h.

Solutions for activation were prepared using tin(II) chloride dihydrate (Aldrich, 98%, ACS reagent grade) and palladium(II) chloride (Alfa Aesar, 99.9%). Two solutions were prepared by dissolving 0.1 g/L of each of these salts in 0.01 M HCl. The activation procedure consisted of first dipping the substrate in the tin chloride solution and then in palladium chloride solution with intermediate rinsing in DI water between the solutions. This cycle was repeated as needed, normally 3−6 times. After activation Pd was deposited for durations of 90 min using the Pd bath composition shown in Table 1. Between each plating, the coated substrate was cooled to room temperature, washed with DI water, and placed in a fresh plating solution for further deposition. No plating was performed after 3−4 platings, due to the deactivation of the support. The membrane was washed and dried overnight at 120 °C. Producing a dense membrane required the repetition of the above-described procedure. Additional details regarding the activation and plating steps can be found elsewhere.[22] Ag and Cu were also deposited on activated Pd by the use of the electroless plating procedure. Chemicals used and the compositions of the plating baths for the Pd, Ag, and Cu deposition are summarized in Table 1.

2.2. Procedures. The thickness of the deposited metal was determined by the gravimetric method, the weight gain of the sample divided by the product of the plated surface area and the metal density. This method gave an average thickness value for the membrane in good agreement with the thickness determined from SEM micrographs.

Surface characterization was performed using an Amray 1610 turbo scanning electron microscope (SEM) equipped with a Princeton Gamma-Tech Avalon EDS

Table 2. Percent of Sample Weight Gain and Flux Change after Oxidation

sample	T_{ox} (°C)	Δm (%)	D_p (μm)	t_{hom} (μm)	t_{ex} (μm)	ΔJ (%)[26]
1	25	unoxidized	3.9			0.0
2	400	0.03	4.1	0.002	0.20	0.0
3	600	0.56	3.9	0.027	3.29	−10.4
4	800	1.47	3.7	0.070	8.61	−73.5

light element detector for the qualitative and quantitative analysis. The spatial resolution for SEM-EDS lies between 0.8 and 1.2 μm for the samples we investigated. SEM specimens of the metal deposited porous stainless steel supports were cut using a SiC saw blade and mounted with phenolic powder in a Smithells II mounting press. Resulting samples were ground with SiC papers with increasing grain fineness from 80 to 400 grit. Grinding was performed by using Metaserv 2000 grinder−polisher. Vibromet I automatic polisher was used to polish the sample to 1 μm overnight. Prior to SEM cross-section analysis, samples were sputter coated using a gold/palladium target to avoid charging.

3. Results and Discussion

3.1. Effects of Oxidation Temperature on Oxide Barrier Layer. Table 2 summarizes the change of the properties of the 0.5 μm grade PSS supports after oxidation at various temperatures. These properties include the He flux ΔJ after oxidation as a percentage of the original He flux for the support and the mean pore diameter, D_p, from Hg porosimetry.[26] The mass gain, Δm, was given as a percentage of the original mass. The changes in mass during oxidation were used to determine the upper and lower bounds of the oxide layer thickness on the basis of two limiting cases for oxide distribution. For the lower bound, the oxide layer was assumed to form a film of uniform thickness on the entire surface area, including the pore walls. This limiting case is referred to as the homogeneous oxide thickness, t_{hom}. The surface area for the 0.5 μm PSS was estimated to be 0.041 $m^2\ g^{-1}$ using Hg porosimetry data. This value was used with the sample mass data to determine the total oxide film area for each sample for the homogeneous oxide case. The upper bound for the oxide thickness, t_{ex}, was estimated by assuming the oxide layer formed entirely on the exterior surface for each plate (2.4 cm^2). For each case a density of 5.1 g/cm^3 was assumed to approximate the density of our oxides on the basis of the work of Adachi et al.[27]

As can be seen from Table 2, weight gains of the samples increase with the oxidation temperature indicating the formation of a thicker oxide layer at higher temperatures. However, the oxidation had little effect on the mean pore size indicating that oxidation did not constrict the internal pore system even at 800 °C. The estimated homogeneous oxide layer thickness values are 2−3 orders of magnitude smaller than the mean pore diameters indicated by Hg porosimetry (3.7−4.1 μm). On the basis of this comparison, the dramatic decrease of the He flux in Table 2 cannot be explained by the formation of a homogeneous oxide layer throughout the pore system, especially for high oxidation temperatures. However, the thickness estimates obtained by assuming oxidation only on the exterior (t_{ex}) were greater than the thickness estimates determined by the cross-sectional SEM analysis that will be discussed later. This difference was less than 1 order of magnitude in all cases. One possible explanation for all of these observations is the predominant formation of oxide on both the exterior surface and in the pores and pore mouths near the surface. The fact that the difference in the pore size distribution between the oxidized and unoxidized support is negligible not only further substantiates this explanation but also gives a clear indication that no pore collapses occurred during the oxidation. Therefore, the mechanical strength of the support is not compromised by the oxidation.

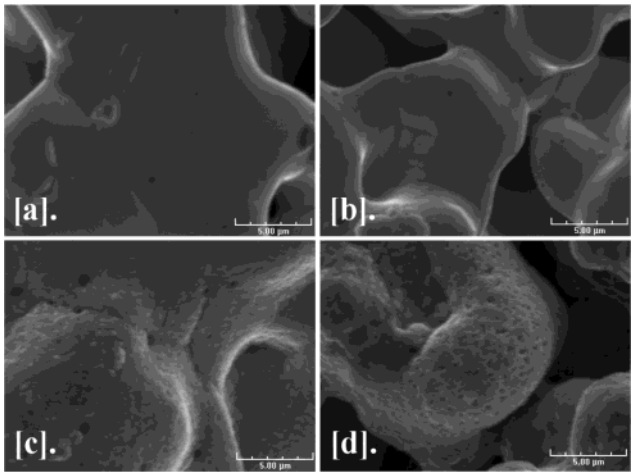

Figure 1. SEM micrographs (5K×) of the supports after oxidation: (a) unoxidized; (b) oxidized at 400 °C; (c) oxidized at 600 °C; (d) oxidized at 800 °C.

Figure 1 shows the SEM micrographs of the PSS surface after oxidation at various temperatures. It can be seen that the surface of sample 1, unoxidized, and sample 2, oxidized at 400 °C, look smooth and similar, whereas the surfaces of samples 3 and 4, oxidized at 600 and 800 °C, respectively, are much rougher. For sample 4, the surface was very crumbly and the roughness seemed to increase substantially compared to the unoxidized sample.

Figure 2 shows the EDS spectrum on the surface of the sample oxidized at 600 °C. The oxygen peak observed on the left confirms the formation of an oxide layer on the support. It was also observed that the amount of oxygen on the support was increasing with higher oxidation temperatures indicating a thicker oxide layer, consistent with the weight uptakes.

Among the oxides that can be formed with the elements of stainless steel, Cr_2O_3 is the most stable oxide due to its low Gibbs free energy, the low diffusion rates of elements in the oxide scale, and its high chemical stability under a H_2 atmosphere.[28] Therefore, it is the most desirable oxide phase for use as a barrier layer to intermetallic diffusion. To check the existence of a Cr-rich oxide on the surface of the samples, EDS spot scan analysis was performed. The ratio of atomic Fe to atomic Cr on the surface of the supports is shown in Figure 3. The ratio remained almost constant and essentially the same as the unoxidized sample for the samples oxidized at 400 and 600 °C whereas it increased dramatically for the support oxidized at 800 °C indicating an Fe-rich oxide on the outermost layer. However, it was difficult to determine the compositions of the oxide layers for samples oxidized at 400 and 600 °C because the thickness of the oxide layer was too thin to be accurately determined due to the limitation of the resolution of the EDS. Chromium oxide was likely

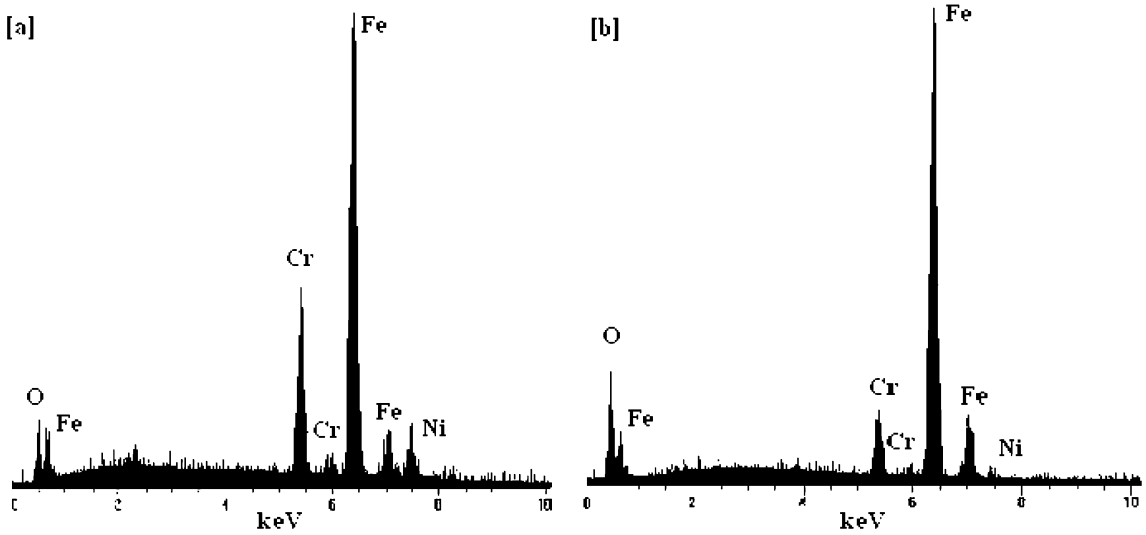

Figure 2. EDS spectra (a) for sample 3, oxidized at 600 °C, and (b) for sample 4, oxidized at 800 °C.

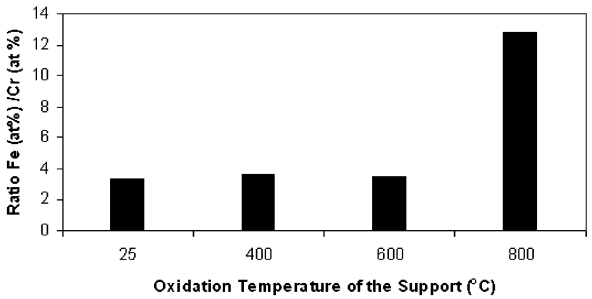

Figure 3. Ratio of Fe (at. %)/Cr (at. %) obtained from EDS spot scan analysis on the surface of the supports oxidized at various temperatures.

formed on the samples at these temperatures due to its low Gibbs free energy. On the other hand, the enhancement of the diffusion of Fe at higher oxidation temperatures could have led to the growth of iron oxide on the chromium oxide layer during oxidation at 800 °C.[28]

To determine the effectiveness of the oxide layer as an intermetallic diffusion barrier, the four samples were electroless plated with Pd and then annealed at 550 °C for 10 h under He atmosphere. Figures 4 and 5 show respectively the SEM micrographs of the cross sections and the corresponding EDS line scan data for the samples oxidized at 400 and 800 °C after annealing. The line scans were performed starting from inside the support, which was darker in color, and ending inside the Pd layer which was lighter. Regions where the line scan data were taken are indicated by the arrows.

For the unoxidized support and the support oxidized at 400 °C (Figure 4) neither the SEM micrographs nor the EDS line scan data conclusively showed the oxide layer, which might have been too thin to even be detected by the EDS line scan. The diffusion of support elements into the Pd layer appears to be similar for both samples.

From the cross-sectional SEM micrograph of sample 3 (not shown), oxidized at 600 °C, a dark uniform thin layer between the support and Pd layer was observed throughout the whole support. Both the EDS line scan on the cross section and the EDS spot scan on the surface confirmed that this dark layer was actually the oxide layer. The thickness of this layer was about 0.2−0.3 μm from the secondary electron image (SEI) micro-

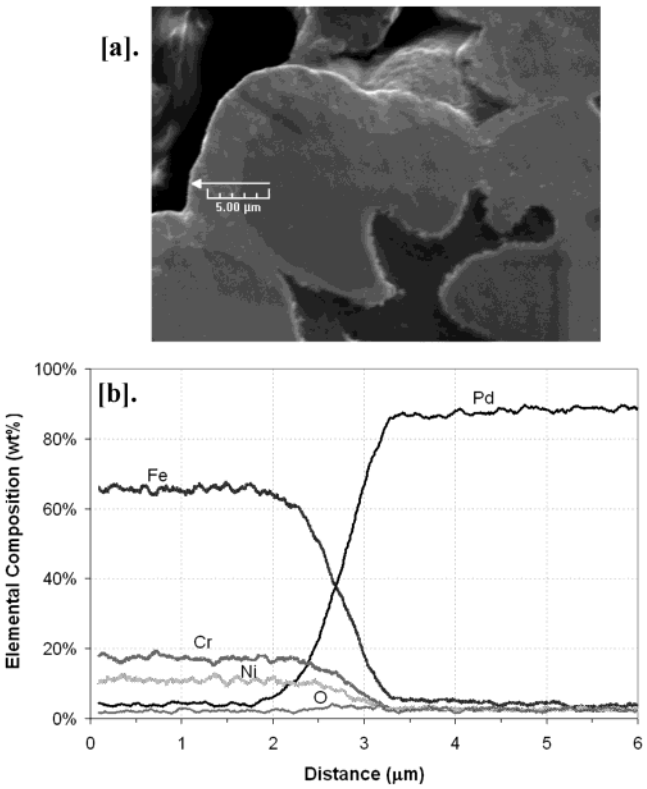

Figure 4. (a) SEM micrograph (5K×) of the cross section of sample 2, support oxidized at 400 °C and annealed at 550 °C under helium atmosphere. (b) EDS composition profile along the length of the arrow indicated in (a).

graph. This was too close to the spatial resolution of the EDS to determine an oxide-only composition.

Figure 5 shows the SEM micrograph and EDS line scan data for sample 4, which was oxidized at 800 °C. A thicker dark region with a very nonuniform thickness was observed throughout the whole plate. It could also be observed that the surface of this oxide layer was very crumbly (Figure 1d). In the cross section of this sample the Pd penetrated deeply into all the cavities of the oxide layer; therefore, the adhesion of the Pd layer might also be enhanced by the formation of this oxide layer. The thickness of the dark region varied from 1 to 6 μm from spot to spot. Since the oxide layer was relatively thick

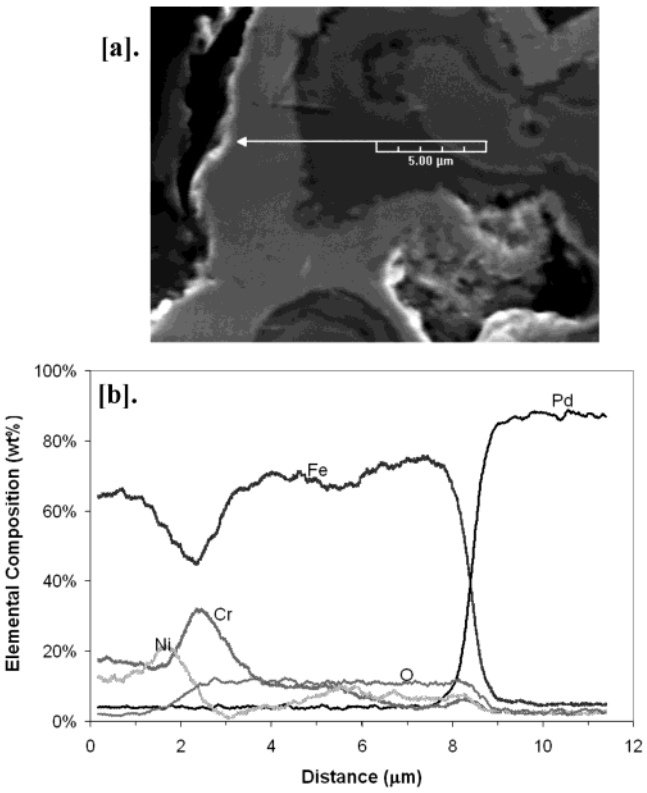

Figure 5. (a) SEM micrograph (5K×) of the cross section of sample 4, support oxidized at 800 °C and annealed at 550 °C under helium atmosphere. (b) EDS composition profile along the length of the arrow indicated in (a).

in this case, it was possible to determine the composition by EDS analysis. It can be seen that there existed an Fe-rich oxide on the outermost layer whereas there was an Fe-depleted and a Cr-enriched mixed oxide on the inner layer. These data agree well with the results reported by Tanabe and Imoto[29] and are consistent with our determined mass gains and spot scans on the surface.

In general, the oxidation process consists of two main steps, surface oxidation and then the oxide scale formation. During the oxide scale formation there are several mechanisms including the diffusion of elements along their respective gradients, the diffusion of oxygen and oxidation at the metal oxide interface. All these mechanisms may affect the composition and the thickness of the formed oxide layer.[30] Considering the fact that the Tamman temperature of 316L stainless steel, above which the elements become mobile, is about 550 °C, for relatively low oxidation temperatures such as 400 °C, it is most likely that only surface oxidation step takes place. For the sample oxidized at 400 °C, the very low mass gain after oxidation, the similarity of the surface morphology to that of the unoxidized sample, and the cross-sectional SEM and EDS results all suggest that the oxide layer formed was very thin. For this case where the oxidation temperature was well below the Tamman temperature, the oxide was probably in the nanometer scale and, therefore, could not be detected by using SEM or EDS. This was consistent with Shibagaki et al.,[31] who using μAES reported a 16 nm thick oxide layer on 316L stainless steel after oxidation at 427 °C under air. The existence of an oxide layer and the growth of this oxide layer with increasing oxidation temperatures have been reported by many authors.[29,31,32] For high oxidation temperatures such as 800 °C, the thick oxide layer consisted of an Fe-rich oxide layer on top followed by a mixed Cr and Fe oxide layer.[29,32] Tanabe and Imoto[29] used SEM to show the lavalike iron oxide on SUS 316 type stainless steel after oxidation at 800 °C in air. Their SEM micrographs of iron oxide on the surface were very similar to what we observed. However, for lower oxidation temperatures there were different results reported by different authors in the literature. For example, Sivaraman et al.[32] reported the oxide layer consisted of Cr_2O_3 after oxidation at 700 °C in air whereas Shibagaki et al.[31] reported an Fe-rich top layer after oxidation at 427 °C in air. These differences might have arisen from the difficulty in the analysis of the thin oxide layer.

Independent of the composition, the most important feature for the oxide layer to be used as a barrier layer for Pd/PSS membranes is its stability under H_2 atmosphere. It is known that most of the oxides are reduced to metallic state under H_2 atmosphere. No reduction will occur on the oxide−metal interface if the inner oxide layer consists of Cr-rich phase which has a high resistance to reduction under H_2 atmosphere even at high temperatures.[28] In this case, even if the inner oxide layer is an Fe-rich phase and reduction occurs, the effectiveness of the barrier layer will not be compromised because of the presence of the stable chromium oxide phase. The line scan results shown in Figures 4 and 5 appear to, at least, qualitatively substantiate the fact that the intermetallic diffusion between the substrate metals and Pd layer has been minimized with the presence of the oxide barrier layer.

3.2. Surface Morphological Changes during Membrane Synthesis. As discussed in the Experimental Section, alloy membrane synthesis consisted of successive steps such as cleaning and oxidation of the PSS support, activation, and electroless plating of Pd, Ag, or Cu. SEM micrographs showing the morphological changes during the synthesis starting with the bare support are given in Figure 6. The bare 0.5 μm support is shown in Figure 6a,b immediately following cleaning and after 6 h of oxidation at 400 °C, respectively. The oxidized supports are typically rougher than the unoxidized supports. However this effect is far less visible for samples oxidized at 400 °C than for those oxidized at 600 and 800 °C, as shown in Figure 1. In both Figure 6a,b the sintered particles which form the PSS support are clearly visible. The gaps and holes between these particles are also visible ranging in size from 2 to10 μm. This is consistent with the mean pore diameter of 3.7−4.1 μm determined by Hg porosimetry shown in Table 2. Little change is apparent upon activation as shown in Figure 6c. The activation process seeds the surface of the support with Pd nuclei which are on the nanometer scale, and these features are too small to be definitively identified by the SEM used in these studies.

The typical surface morphologies obtained by electroless plating of Pd, Ag, and Cu are shown in Figure 6d−f. Figure 6d shows Pd-plated surface of a PSS support which was prepared using the steps illustrated in Figure 6a−c. This sample is shown after only preliminary plating and was not covered by a gastight layer of Pd. The Pd covers the entire support surface with a uniform layer of tightly knit clusters which are 1 μm and smaller. The Pd coverage may be seen to penetrate into every valley and crevasse for which the bottom surface or walls are visible. The uniformity of

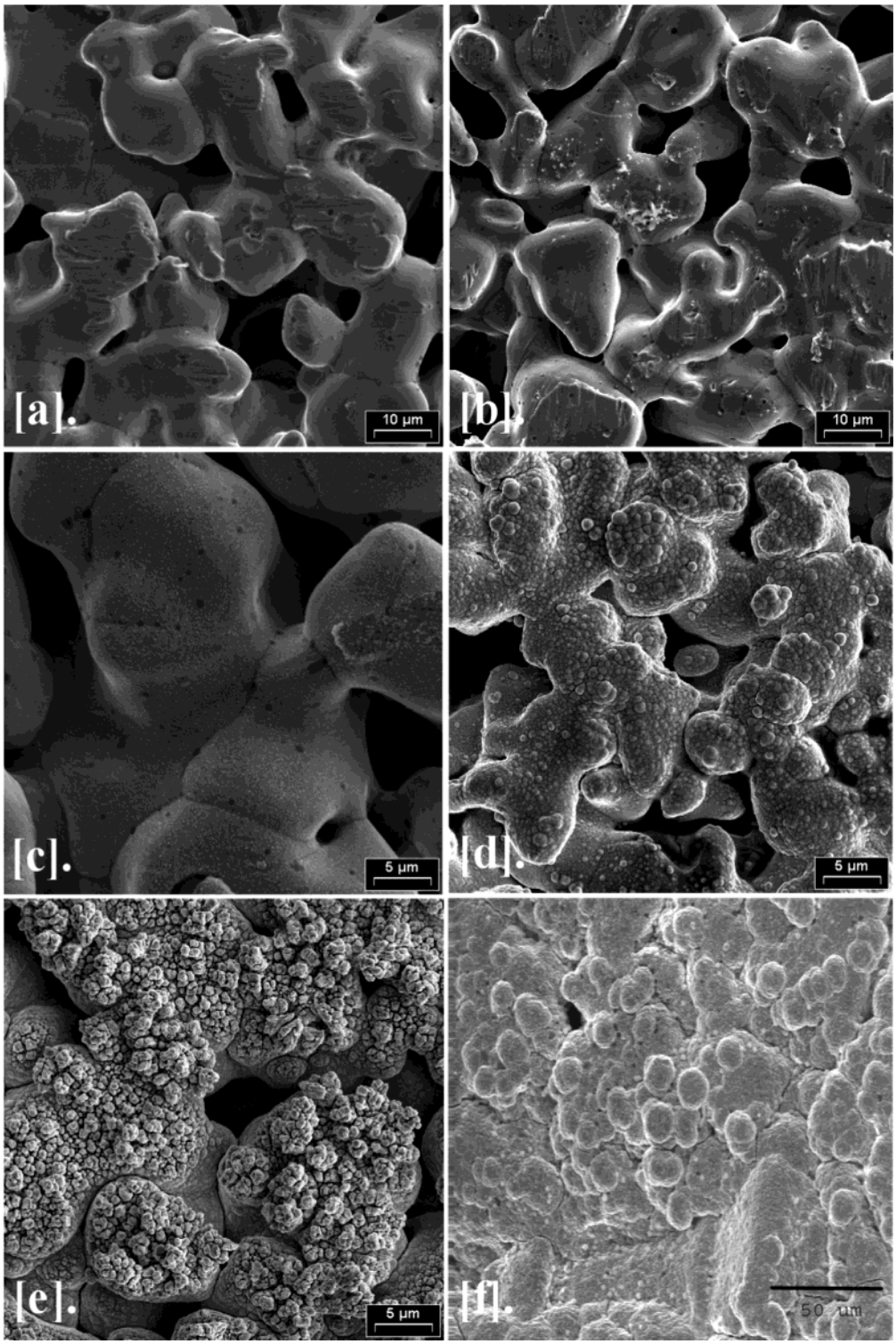

Figure 6. Morphological changes during membrane fabrication: (a) bare PSS support after cleaning (1K×); (b) PSS support oxidized at 400 °C for 6 h (1K×); (c) oxidized and activated PSS support (2K×); (d) Pd-plated PSS support surface (2K×); (e) Pd + Ag plated PSS support surface (2K×); (f) Pd + Cu plated PSS support surface (500×).

electroless Pd deposits and the penetration into surface topological features are general characteristics of the electroless plating of Pd on PSS supports which have been noted by Mardilovich et al.[25] In addition, our previous work showed that the electroless plating methods were effective in covering macroscopic defects such as dents, tool marks and abrasions, and transitions in the substrate such as the weld and other topological features such as the curvature of the support and the deposited dense Pd layer simply conformed to the original surface topology.[33] The thinnest membrane we were able to synthesize with the current commercially available porous stainless steel substrate was 11.7 μm.

For this work, the alloying metals, Ag and Cu, were plated only after initial plating of Pd on the PSS support. Figure 6e,f shows surface layers of Ag and Cu, respectively, plated on an activated surface that was first plated with Pd. The composite layers shown in these figures have not been annealed. The deposition of Ag on Pd led to a heterogeneous rough surface

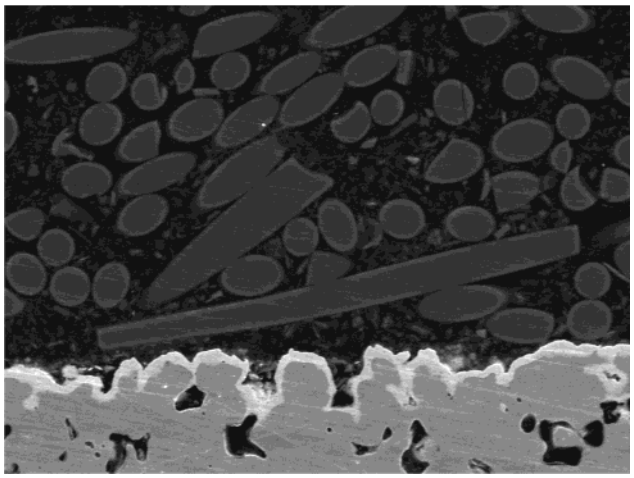

Figure 7. Cross-section view of Pd−Ag−PSS composite plate, annealed at 600 °C for 10 h (600×).

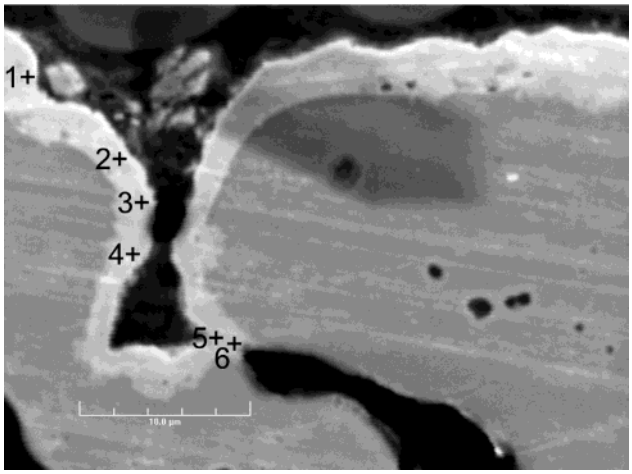

Figure 8. SEM micrograph for the annealed Pd−Ag layer in the region of a large pore opening in the support. Locations for EDS spot scans (see Figure 9) have been indicated by numbered crosses (3K×).

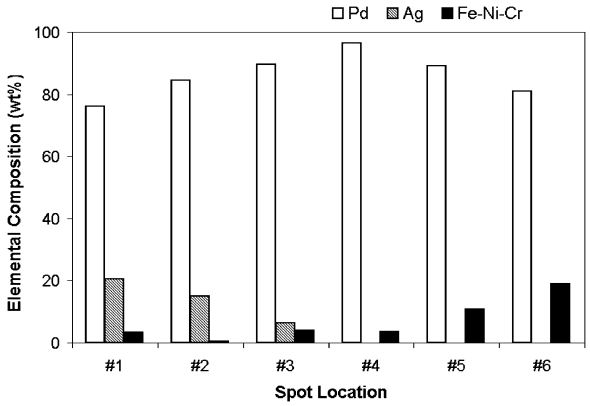

Figure 9. EDS spot scan compositions for points indicated in Figure 8. Data for the support metals are the sum of the compositions for Fe, Ni, and Cr.

coverage. The particles of Ag in this layer tended to form clusters which grew in the direction normal to the surface. It is interesting to note that the Ag layer did not seem to penetrate the pore mouths and valleys. The bottoms and internal walls of the support (where visible) in Figure 6e had a surface morphology which was similar to the surfaces in Figure 6d, indicating that these portions were predominantly covered by Pd. Finally, Figure 6f shows that the plating of Cu on Pd led to a surface which was uniformly covered by spherical agglomerates of Pd/Cu clusters, which were about 10 μm in size. It should be noted that the surface shown in Figure 6f is that of a membrane which was very close to being gastight and, therefore, the cavities and surface topology of the support are no longer visible.

3.3. Annealing of Pd−Ag Multilayers Formed by Sequential Deposition. To evaluate the formation of Pd−Ag alloy layers, a 2.4 μm Pd layer was applied first to an activated 0.5 μm PSS support followed by a 0.75 μm Ag layer. The support was oxidized at 400 °C for 10 h before the plating of the metals. The resulting Pd−Ag−PSS composite was annealed at 600 °C for 10 h in helium. Figure 7 shows a typical cross-section SEM micrograph of the sample after annealing.

The upper dark portion and lower gray regions correspond to the phenolic mounting material and the porous stainless steel, respectively. The thin palladium and silver layer lies between these two regions and is light gray in the micrograph. As can be seen from Figure 7, the Pd−Ag layer appeared to form a uniform thin layer on the PSS substrate, covering small gaps of the porous layer and even depositing into the large openings in the support which ranged 10−20 μm in width and 15−25 μm in depth.

EDS spot scans were performed at various points in the layer to determine if a uniform alloy was produced by annealing. Figure 8 shows an SEM micrograph of the annealed Pd−Ag layer in the region of a large pore opening in the support with indication of the location of several EDS spot scans. The elemental compositions of Pd, Ag, and support metals (Fe, Ni, and Cr) obtained from these spot scans are presented in Figure 9. In the order from spot number 1 in the upper left corner of Figure 8 and descending into the pore along the left wall to spot number 4, there is a steady decrease in Ag content and a steady increase in Pd as shown in Figure 9. The three spots located in the deepest section of the large pore (spots 4−6) have almost no Ag. This indicates that Ag was not deposited inside the pores and openings during plating, as was observed in Figure 6e. The heterogeneous nature of the Ag deposition process may present an additional challenge to attaining a homogeneous alloy membrane on these PSS supports.

An additional point of interest in Figure 8 is the small pore opening at the bottom right of the larger pore. This small pore appears to have been closed in the plating process. The amount of the diffusion of the support metals (Fe, Ni and Cr) into this region (spots 5 and 6) appeared to be greater than that in the other regions. This might have resulted from the fact that this region had support walls in close proximity on all but two sides. It was noted in a previous section that the in-situ oxidation process led to an oxide coverage that was predominantly on and near the surface of the support. Therefore, it is also possible that the oxide coverage in this small pore beneath the surface was insufficient to protect the alloy layer from intermetallic diffusion in these locations. The apparent increase in the intermetallic diffusion at these points could significantly reduce the hydrogen permeability and is therefore in need of further study.

3.4. Pd−Cu Alloy Formation at 500 and 600 °C. A 0.5 μm PSS support was cleaned and oxidized at 430 °C for 8 h before Pd and Cu deposition. The bimetallic film was composed of 12 μm of Pd plated on the support and 12 μm of Cu plated on top of the Pd layer. This

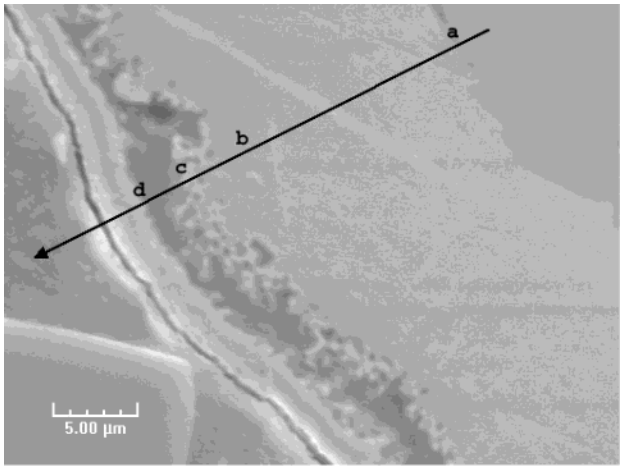

Figure 10. SEM micrograph of the cross section of the membrane after heat treatment at 500 °C. The arrow indicates the length and direction of the EDS composition profile analysis performed on this sample (3K×).

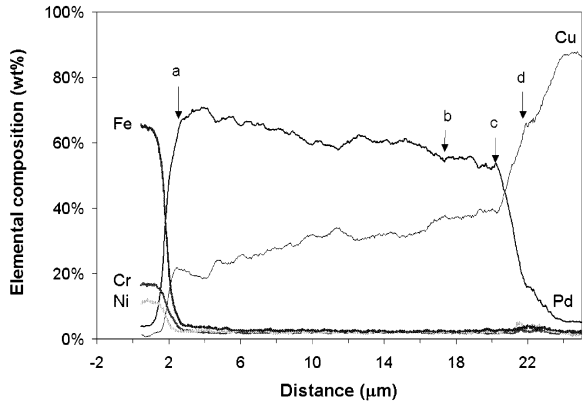

Figure 11. Composition profile of different elements along the arrow in Figure 10 by EDS line scan.

composite was annealed at 500 °C for 120 h under helium. Figure 10 shows an SEM micrograph of the bimetallic Pd/Cu layer after annealing. An arrow has been superimposed on the figure which starts in the PSS support on the upper right side, passes through the Pd/Cu layer, and ends in the sample mounting material. The EDS composition profile shown in Figure 11 was taken along the length of this arrow. Three different regions can be seen in the Pd/Cu film in Figure 10. The first region is an 18−19 μm thick gray layer which borders the support and is designated by points a and c in Figure 11. The second region is a 1−2 μm dark layer designated by the points c and d. Finally the third region is a 2 μm gray layer on the outer edge of the membrane, for which the Pd compositions are given to the left of the marker d.

The first region is the Pd-rich portion of the membrane. The Pd content of the first region decreased slowly from around 80 wt % (point a, Figure 11), at the Pd−PSS interface, to around 60 wt % at point c. The second and third regions comprise the Cu-rich portion of the membrane. In the second region the Pd content decreased rapidly to a value close to 17−18 wt % at point d. The third region is the remainder of the original Cu layer into which some Pd has diffused. The Pd content in this layer decreased from 18 wt % at point d to 10 wt % at the membrane surface.

The Pd/Cu interface was originally situated at 12 μm from the Pd−PSS interface. After heat treatment the

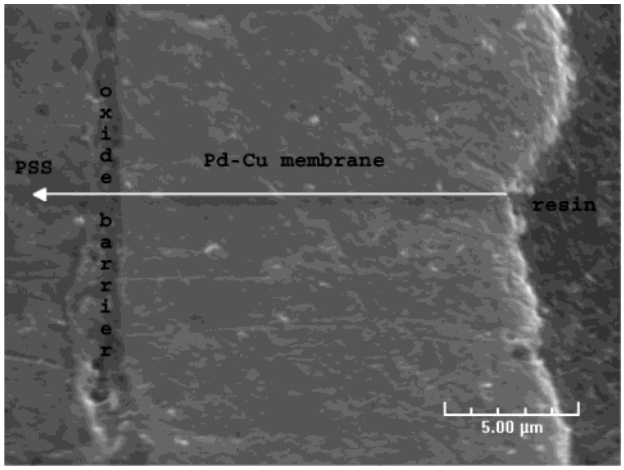

Figure 12. Pd/Cu film on PSS support oxidized at 800 °C for 10 h after annealing. Heat treatment was carried out at 600 °C for 10 h under helium (3K×).

interface between the Pd-rich portion and start of the Cu-rich portion of the membrane (point c) was located at 18−19 μm from the Pd−PSS interface. Figure 11 indicates that the Pd-rich portion of the membrane near the interface marked by point c is close in composition to the expected range for the β phase bcc Pd/Cu alloy. At 500 °C the stability domain of the β phase lies between 46 and 56 Pd wt %.[34] The region where Pd concentration is within the β phase limits is between points b and c in Figure 11. The diffusion of Pd and other metals is known to occur much faster in β-Pd/Cu than in the more Pd-enriched α-phase alloy.[35] The 6−7 μm shift of the interface between the Pd-rich portion of the membrane toward the Cu rich portion resulted from the faster diffusion of Pd in the β-Pd/Cu phase than in the α-Pd/Cu phase, in agreement with Butrymowicz et al.[35]

The Pd concentration of the thin dark second region in the micrograph varied from around 54 wt % at point c to 18 wt % at point d. These values correspond to Pd/Cu alloys characterized by a short-range order. Their likely crystal structure was fcc. The last layer starting at point d was the Cu rich α phase.

The alloying process of 12 μm thick layers was very slow at 500 °C, and to reach uniformity several hundred hours would be needed. Therefore, higher temperatures were considered.

The support used for the heat treatment at 600 °C was a 0.5 μm PSS cup that was cleaned and oxidized at 800 °C for 10 h prior to plating. The bimetallic film was composed of 10 μm of Pd covered by 5 μm of Cu and was annealed at 600 °C for 10 h under helium. Figure 12 shows the Pd/Cu alloy film after heat treatment.

The PSS support is on the left side and the Pd/Cu thin film is on the right side. A thin layer can be noticed between the support and the alloy film. This mixed Fe−Cr oxide layer resulted from the oxidation process at 800 °C. The EDS analysis of the annealed membrane (Figure 13) shows an almost uniform Pd-rich alloy. Furthermore, Fe, Ni, and Cr cannot be seen in the Pd/Cu alloy film near the support, indicating minimum intermetallic diffusion between the elements in the substrate and Pd/Cu layer.

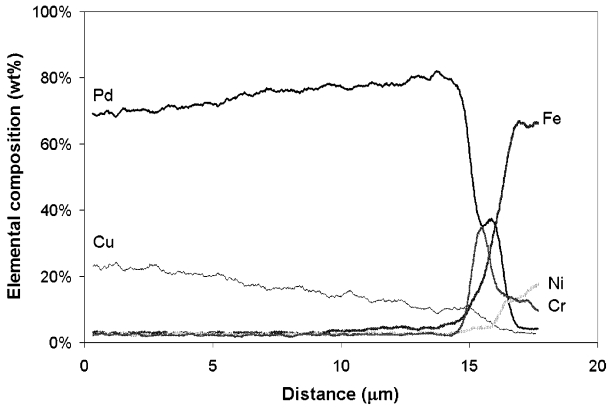

Figure 13. Compositions profiles of different elements along the arrow in Figure 12 by EDS line scan.

4. Conclusions

The formation of an oxide layer as the intermetallic diffusion barrier for composite Pd−, Pd/Ag−, and Pd/Cu−porous stainless steel membranes has been investigated by examining the morphological changes of the porous stainless support by SEM and EDS after oxidation in air. Although, for relatively low oxidation temperatures, the oxide layer was too thin to be detected by SEM or EDS, both mass uptakes and cross sectional SEM and EDS analyses showed a uniform thin oxide layer at intermediate temperatures around 600 °C and a crumbly, thick oxide layer at high temperatures such as 800 °C. SEM and EDS results from Pd, Pd/Ag, and Pd/Cu membranes annealed at different temperatures showed the oxide layer to be an effective intermetallic barrier. The temperature that the barrier was stable depends on the temperature at which the substrate was oxidized.

Results from the annealing study for the formation of the Pd/Ag alloy membrane at 600 °C showed that the temperature was insufficient to form a uniform alloy membrane. Furthermore, the nonuniform Ag deposition characteristics of being difficult to deposit in the pores and valleys of the substrate could also make the formation of a uniform alloy membrane challenging and require further understanding of the plating mechanisms and kinetics.

Since no impurities, such as Fe, Ni, and Cr, were detected in the Pd/Cu alloy membrane at the PSS−membrane interface at 500 °C, the barrier layer formed by the oxidation of the substrate at 430 °C was effective in reducing the intermetallic diffusion at 500 °C. However, this temperature was insufficient for the formation of a uniform Pd/Cu alloy from a 12 μm Pd layer and 12 μm Cu layer. Yet, after annealing of the samples at 600 °C for 10 h for a 10 μm Pd layer and 5 μm Cu layer, a very uniform Pd/Cu alloy membrane was formed on a substrate oxidized at 800 °C.

Acknowledgment

The financial support provided by Shell International Exploration and Production Inc. is gratefully acknowledged.

Literature Cited

(1) United States Department of Energy. National Hydrogen Energy Road map, Based on the results of the National Hydrogen Energy Road map Workshop; Washington, DC, 2002.

(2) Barreto, L.; Makihira, A.; Riahi, K. The hydrogen economy in the 21st century: a sustainable development scenario. *Int. J. Hydrogen Energy* **2003**, *28*, 267.

(3) Fishtik, I.; Datta, R. Personal communication.

(4) Matzakos, A. N.; Wellington, S. L.; Mikus, T.; Ward, J. M. Integrated flameless distributed combustion/steam reforming membrane reactor for hydrogen production and use thereof in zero emissions hybrid power system. U.S. Patent Application, U.S. 2003/0068269 A1, 2003.

(5) Wellington, S. L.; Matzakos, A. N.; Mikus, T.; Ward, J. M. Integrated flameless distributed combustion/membrane steam reforming reactor and zero emissions hybrid power system. U.S. Patent Application, U.S. 2003/0068260 A1, 2003.

(6) Uemiya, S.; Sato, N.; Ando, H.; Kude, Y.; Matsuda, T.; Kikuchi, E. Separation of hydrogen through palladium thin film supported on a porous glass tube. *J. Membr. Sci.* **1991**, *56*, 303.

(7) Jayaraman, V.; Lin, Y. S. Synthesis and hydrogen permeation properties of ultrathin palladium−silver alloy membranes. *J. Membr. Sci.* **1995**, *104*, 241.

(8) Mardilovich, P. P.; She, Y.; Ma, Y. H.; Rei, M. H. Defect free palladium membrane on porous stainless steel support. *AIChE J.* **1998**, *44* (2), 310.

(9) Cheng, Y. K.; Yeung, K. P. Palladium−silver membranes by electroless plating technique. *J. Membr. Sci.* **1999**, *158*, 127.

(10) Tosti, S.; Bettinali, L.; Violante, V. Rolled thin Pd and Pd−Ag membranes for hydrogen separation and production. *Int. J. Hydrogen Energy* **2000**, *25*, 319.

(11) Keuler, J. N.; Lorenzen, L. Developing a heating procedure to optimize hydrogen permeance through Pd−Ag membranes of thickness less than 2.2 μm. *J. Membr. Sci.* **2002**, *195*, 203.

(12) Ozaki, T.; Zhang, Y.; Komaki, M.; Nishimura, C. Preparation of palladium-coated V and V-15Ni membranes for hydrogen purification by electroless plating technique. *Int. J. Hydrogen Energy* **2003**, *28*, 297.

(13) Shu, J.; Grandjean, B. P. A.; Ghali, E.; Kaliaguine, S. Simultaneous deposition of Pd and Ag on porous stainless steel by electroless plating. *J. Membr. Sci.* **1993**, *77*, 181.

(14) Li, Z. Y.; Maeda, H.; Kusakabe, K.; Morooka, S.; Anzai, H.; Akiyama, S. Preparation of palladium−silver membranes for hydrogen separation by the spray pyrolysis method. *J. Membr. Sci.* **1993**, *78*, 247.

(15) Souleimanova, R. S.; Mukasyan, A. S.; Varma, A. Effects of osmosis on microstructure of Pd-composite membranes synthesized by electroless plating technique. *J. Membr. Sci.* **2000**, *166*, 249.

(16) Edlund, D. J.; McCarthy, J. The relationship between intermetallic diffusion and flux decline in composite-metal membranes: implications for achieving long membrane lifetime. *J. Membr. Sci.* **1995**, *107* (1−2), 147.

(17) McKinley, D. L. U.S. Patent 3,439,474, 1969.

(18) Karpova, R. A.; Tverdovskii, I. P. Hydrogen sorption in the dispersed palladium−copper alloys. *Zh. Fiz. Khim.* **1959**, *33*, 1393.

(19) McKinley, D. L. U.S. Patent 3,350,845, 1967.

(20) Roa, F.; Way, J. D.; McCornick, R. L.; Paglieri, S. N. Preparation and characterization of Pd−Cu composite membranes for hydrogen separation. *Chem. Eng. J.* **2003**, *93*, 11.

(21) Nam, S. E.; Lee, K. H. Hydrogen separation by Pd alloy composite membranes: introduction of diffusion barrier. *J. Membr. Sci.* **2001**, *192*, 177.

(22) Ma, Y. H.; Mardilovich, P. P.; She, Y. U.S. Patent 6,152,987, 2000.

(23) Mardilovich, P. P.; She, Y.; Ma, Y. H.; Rei M. H. Stability of hydrogen flux through Pd/porous stainless steel composite membranes. *Proc. Fifth Int. Conf. Inorg. Membr.* **1998**, *1*, 246.

(24) Rubow, K. L.; Strange, L. Sintered Porous Metal Filtration Systems for Petroleum Refining Applications. *AFS 2002 Annual Technical Conference and Exposition*, Galveston, TX, 2002.

(25) Mardilovich, I. P.; Engwall, E. E.; Ma, Y. H. Dependence of hydrogen flux on the pore size and plating surface topology of asymmetric Pd-porous stainless steel membranes. *Desalination* **2002**, *144*, 85.

(26) Akis, B. C.; Engwall, E. E.; Mardilovich, I. P.; Ma, Y. H. Effects of the in-situ formation of an intermetallic diffusion barrier layer on the properties of composite Palladium membranes. *ACS Prepr.* **2003**, *48* (1), 337.

(27) Adachi, I. *Trans. Iron Steel Inst. Jpn.* **1996**, *6*, 118.

(28) Samsanov, G. V. *The Oxide Handbook*; IFI/Plenum: New York, Washington, DC, London, 1973.

(29) Tanabe, T.; Imoto, S. Surface oxidation of type 316 stainless steel. *Trans. JIM* **1979**, 20.

(30) Shackelford, J. F. *Introduction to Materials Science for Engineers*; Prentice Hall: Upper Saddle River, NJ, 1996.

(31) Shibagaki, S.; Koga, A.; Shirakawa, Y.; Onishi, H.; Yokokawa, H.; Tanaka, J. Chemical reaction path for thin film oxidation of stainless steel. *Thin Solid Films* **1997**, *303*, 101.

(32) Sivaraman, G.; Raj, B.; Jayakumar, T. Oxidation behaviour of type 316 stainless steel in the temperature range 873−1073K. *Trans. Indian Inst. Met.* **1984**, *37*, 3.

(33) Ma, Y. H.; Mardilovich, I. P.; Engwall, E. Thin Composite Palladium and Palladium/Alloy Membranes for Hydrogen Separation. *Ann. N.Y. Acad. Sci.* **2003**, *984*, 346.

(34) Subramanian, P. R.; Laughlin, D. E. Cu−Pd (Copper−Palladium). *J. Phase Equilib.* **1991**, *12*−*2*, 231.

(35) Butrymowicz, D. B.; Manning, J. R.; Read, M. E. Diffusion in copper and copper alloys. *J. Phys. Chem.* **1975**, *5*−*1*, 179.

Received for review July 10, 2003
Revised manuscript received October 16, 2003
Accepted November 6, 2003

IE034002E